Ion adsorption at a metallic electrode: an *ab initio* based simulation study

2009 J. Phys.: Condens. Matter 21 424109

(http://iopscience.iop.org/0953-8984/21/42/424109)

J. Phys.: Condens. Matter **21** (2009) 424109 (11pp) doi:10.1088/0953-8984/21/42/424109

Ion adsorption at a metallic electrode: an *ab initio* based simulation study

M Pounds[1], S Tazi[2], M Salanne[2,3] and P A Madden[4]

[1] School of Chemistry, University of Edinburgh, Edinburgh EH9 3JJ, UK
[2] UPMC Univ Paris 06, UMR 7195, PECSA, F-75005, Paris, France
[3] CNRS, UMR 7195, PECSA, F-75005, Paris, France
[4] Department of Materials, University of Oxford, Parks Road, Oxford OX1 3PH, UK

Received 22 April 2009, in final form 25 May 2009
Published 29 September 2009
Online at stacks.iop.org/JPhysCM/21/424109

Abstract
A method for parametrizing, from first principles density functional theory calculations, a model of the interactions between the ions in an ionic liquid and a metallic (electrode) surface is described. The interaction model includes the induction of dipoles on the ions of the liquid by their mutual interaction and the interaction with the electrode surface as well as the polarization of the metal by the ionic charges and dipoles ('image' interactions). The method is used to obtain a suitable interaction model for a system consisting of a LiCl liquid electrolyte and a solid aluminium electrode. The model is then used in simulations of this system for various values of the electrical potential applied to the electrode. The evolution of the liquid structure at the electrochemical interface with applied potential is followed and the capacitance of the electrochemical interface is measured. The electrolyte is found to exhibit a potential-driven phase transition which involves the commensurate ordering of the electrolyte ions with the electrode surface; this leads to a maximum in the differential capacitance as a function of applied potential. Away from the phase transition the capacitance was found to be independent of the applied potential.

(Some figures in this article are in colour only in the electronic version)

1. Introduction

The properties of an ionic liquid close to an interface are determined by a competition between short-range and Coulombic interactions. A particularly significant situation occurs at the interface with a solid electrode, where the changes in structural and dynamical properties, relative to the bulk, can have a substantial effect on the rates of electrochemical reactions. In this case, in addition to the interactions between the ions themselves, the packing of the ions against the solid surface plays an important role and the electrical potential of the electrode may shift the relative energies of cations and anions. Furthermore, especially for metallic electrodes, the ionic charges will polarize the electrode, giving rise to additional so-called image charge interactions. The conventional description of the electrochemical interface, as used in solution electrochemistry, is based upon the mean-field concepts of Gouy and Chapman and leads to the concept of an electrical double-layer. It is now well recognized that such descriptions are not appropriate for the strong interactions which occur in an ionic liquid and that the local structure and the behaviour of the electrical potentials close to the electrode are qualitatively different to double-layer expectations [1–6].

In order to allow an examination by computer simulation of the altered liquid properties close to the metallic electrode/ionic liquid interface we recently introduced a way of representing a system consisting of a fluid confined between a pair of model metallic electrodes maintained at a controlled electrical potential difference [3]. The system is periodically replicated in the plane parallel to the electrodes. The metallic, constant potential condition is attained by minimizing a suitable energy function with respect to variable charges on the electrode atoms, following a procedure suggested by Siepmann and Sprik in a different context [7]. These atomic charges also respond to the potentials caused by the charges on the ions in the fluid, giving rise to image–charge interactions. The system is a direct realization of the models of the electrochemical interface appearing in text books and the properties of the fluid can be extracted by applying normal statistical mechanical ideas to the molecular dynamics trajectories. It has been used to study the interfacial structure [3] and to model

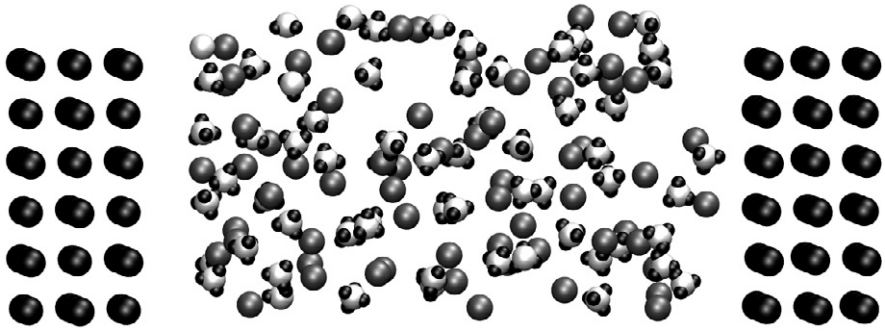

Figure 1. A rendering of the tetragonal distribution of MLWFs (the small black spheres denote the centres of the MLWFs) around each Cl^- ion. The Cl^- ions are coloured white, the Li^+ ions grey, and the wall atoms black. Snapshot obtained with the VMD program [23].

electrochemical charge-transfer involving redox-active ions for aqueous solutions and ionic liquids (molten salts) [8, 9].

In the most recent work on inorganic molten salts, the interactions between the ions are described by polarizable interaction potentials which are parametrized on the basis of *ab initio* electronic structure calculations [10]. Such potentials have been shown to reproduce bulk structural, thermodynamic and transport properties extremely well [11, 12]; they are *predictive* in the sense that no empirical information is used in their construction and highly transferable from pure materials to mixtures. The potentials are constructed by a generalized 'force-matching' method. A suitable condensed-phase ionic configuration is taken from a molecular dynamics simulation using some approximate force field for the material of interest. Typically a hundred ions would be used in periodic boundary conditions. The configuration is then input to a planewave DFT electronic structure program and an energy minimization carried out to find the ground-state electronic structure. From the results of this calculation the force and dipole moment on each ion is obtained, the latter by making use of the transformation of the Kohn–Sham orbitals to a maximally localized Wannier function (MLWF) set. The parameters in the polarizable potential are then optimized by matching the dipoles and forces from the potential on the same ionic configuration to the *ab initio* values [13]. If necessary the process may be iterated, by using the fitted potential to generate a new ionic configuration to input to the *ab initio* calculation. The resulting potentials may be used in much larger scale MD simulations to obtain the physical properties of interest [14, 15]. Implementing such potentials in the electrochemical interface simulations has required the generalization of the previous work to allow the treatment of the interactions between the induced ionic dipoles and the variable charges on the electrode atoms [16].

In this paper we will demonstrate the feasibility of a third step towards realistic simulations of the electrochemical interface in ionic liquids. We will show how the force-matching procedure may be further extended to allow the interactions between the ions of the liquid and the atoms of the metallic electrode to be parametrized from first principles. We will then describe simulations of a system consisting of aluminium metal electrodes and the molten salt LiCl in which all interaction potentials have been obtained on a first principles basis[5]. The simulations were run for several values of the applied electrical potential and the evolution of the structure of the melt close to the interface with changing potential was monitored. The results have been used to calculate the potential dependence of the capacitance of the interfacial region which is, in principle, measurable. These results will be compared with the predictions of beyond-mean-field treatments of the interfacial structure.

2. Parametrization of the electrode–ion interaction potentials

The classical simulations, on which the comparisons with the *ab initio* calculations will be made, involve a cell consisting of 64 Cl^- ions and 64 Li^+ ions, at a density corresponding to the melt at 1200 K, sandwiched between a representation of two parallel slabs of Al. The whole system is periodic in two dimensions and figure 1 illustrates one configuration. The Al slabs consisted of three *fixed* atomic layers, arranged in an fcc geometry, with an interatomic separation equal to 2.01 Å. The x and y dimensions of the cell were both 12.07 Å, and the distance between the atoms in the two outermost layers (i.e. the length of the liquid region) was 21.07 Å. Each atom in the slab interacts with the ions of the liquid via a pair potential and, in addition, carries a variable charge which responds to the local electrical potential due to all the charges and ionic dipoles in the system. A metallic response condition is imposed on these charges by requiring that, at each timestep of the MD simulation, they minimize a functional which ensures that the electrical potential at each atom inside the slab is constant. The atomic charges themselves contribute to the Coulombic forces on the ions in the melt and to the electric fields which induce dipoles on them. The full details of this procedure, which involves a significant extension of that described in [3], are given in [16]. Note that all electrostatic interactions (including dipoles) are treated with a 2d Ewald sum. In these works we have checked that three atomic layers of Al are sufficient to

[5] In reality an Al electrode would melt at the melting temperature of LiCl; this does not happen in our simulations because we do not allow the Al atoms to move. This unphysical system allows us to perform the electronic structure calculations relatively easily because of the small number of valence electrons. A closely related but more realistic system, within the scope of the methods we describe here, would be the LiCl/KCl eutectic mixture with an Al electrode.

reproduce the image–charge effects as predicted by continuum electrostatics for the interaction of point charges with ideally polarizable metallic surfaces [3].

In the initial simulation, to generate a starting configuration for a subsequent *ab initio* calculation, the ions interact with each other via the polarizable potentials described in [12]. The short-range (non-Coulombic) interactions of the ions of the melt with the atoms of the wall were approximated by treating the atoms as if they were additional Cl^- ions [3]. The simulation was initiated by taking a configuration from a run on bulk LiCl and surrounding it with the Al slabs. It was then run for about 10 ps at 1200 K to allow relaxation of the ionic positions. In order to transfer the atomic coordinates from our 2d periodic system bounded by two 3-layer slabs into a 3d periodic *ab initio* code we had arranged the atomic positions in each slab so that when periodicity is introduced in the z-direction, with the appropriate repeat distance, the two 3-layer slabs would join to form a single 6-layer slab of fcc aluminium which, by virtue of the periodic boundary conditions, forms two interfaces with the liquid layer.

We then conducted a short *ab initio* MD run from this starting configuration (which contains 108 Al, 64 Li and 64 Cl atoms) using the CPMD code [17]. The calculations were performed using the PBE exchange–correlation potentials [18] and the Troullier–Martins pseudopotentials [19]. We note that the ability of such a description of the electronic structure to represent the interactions between molecules and ions and a metallic surface has recently been examined by Fernández-Torre *et al* [20]. The $3s^2$ and $3p^5$ electrons are included in the valence set for each Cl atom whilst those in the first and second shells are pseudized; all three electrons of each Li atom are explicitly included in the valence set; and the $3s^2$ and $3p^1$ electrons are included for each Al atom with those in the first two shells pseudized. The planewave cutoff (a kinetic energy cutoff of 952.37 eV on a $128 \times 128 \times 384$ grid) is considerably larger than would normally be used in order to ensure a high degree of convergence of the forces with respect to basis set size.

The final ionic configuration and the associated wavefunction were then retained for analysis. Following Aguado *et al* [10] a Wannier transformation of the Kohn–Sham eigenvectors was applied,

$$w_n(\mathbf{r}) = \sum_{m=1}^{J} U_{nm}|\phi_m\rangle, \tag{1}$$

where the sum runs over all the Kohn–Sham states ϕ_i, and the unitary matrix $\boldsymbol{U}$ was determined by iterative minimization of the Wannier function spread. The Wannier function centre positions were computed through [21, 22]

$$\mathbf{r}_n^\alpha = -\sum_{m=1}^{3} \frac{M_{nm}}{b_m} \Im \ln[U^\dagger K^{(m)} U]_{nm}, \qquad \alpha = x, y, z \tag{2}$$

where $M_{nm} = (\mathbf{b}_n \cdot \mathbf{u}_m)\, b_n^{-1}$ is the normalized projection of the nth reciprocal lattice vector on the mth Cartesian vector, and

$$K_{ij}^{(m)} = \langle\phi_i|\mathrm{e}^{-\mathrm{i}\mathbf{b}_m\cdot\mathbf{r}}|\phi_j\rangle. \tag{3}$$

Figure 1 illustrates for one configuration of this system the positions of MLWFs which lie close to the Cl nuclei. It can be seen that 4 MLWFs (each containing two electrons) are associated with each Cl in a roughly tetrahedral geometry, and a single very tightly localized MLWF is associated with each Li—so the electronic density distribution in the melt is consistent with an ionic picture. It is then straightforward to calculate a dipole moment associated with each ion I using

$$\mu_\alpha^I = -2\sum_{n\in I} r_{n,\alpha} + Z_I R_{I,\alpha} \tag{4}$$

where the sum runs over those MLWFs which are in the vicinity of ion I, and Z_I is the charge of the pseudopotential core at the position $\mathbf{R}_I$.

The output of this run was a set of ionic positions, forces and dipole moments to be used in a force-matching process to determine the short-range, non-Coulombic aspects of the interactions between the ions of the melt and the atoms of the walls. We assume that the 6-atom slab in the *ab initio* calculations is sufficiently thick that the two aluminium surfaces behave independently as regards the Coulombic (image–charge) interactions with the ions in the melt; that is, that each behaves as the surface of a semi-infinite slab of ideally polarizable metal. From this assumption we can extract information on the short-range contributions to the forces and dipoles which may be used in the 2d 'classical' calculations.

2.1. Representation of the ion–electrode polarization interactions

We envision that, in the systems of interest, there is no charge-transfer between the metallic slabs and the ions of the melt. The coulomb and polarization interactions involving the ions of the melt and the atoms of the electrode slabs are represented by the potential

$$\begin{aligned} V = &\sum_{i=1,N}\sum_{j=1,M} (z_i T_{ij}^0 q_j + \boldsymbol{\mu}_i \cdot \mathbf{T}_{ij}^1 q_j + \mathbf{F}_{ij}^{\mathrm{sr}} \cdot \boldsymbol{\mu}_i) \\ &+ V_{\mathrm{MM}}(\{\mathbf{r}_{i=1,N}\}, \{\boldsymbol{\mu}_{i=1,N}\}) \\ &+ V_{\mathrm{EE}}\{q_{j=1,M}\} + V_{\mathrm{M}}^{\mathrm{self}}(\{\boldsymbol{\mu}_{i=1,N}\}) + V_{\mathrm{E}}^{\mathrm{self}}(\{q_{j=1,M}\}), \end{aligned} \tag{5}$$

where the terms within the explicit double sum represent the interactions between the electrode atoms, which carry the variable charges q_j, and the (fixed) charges z_i and (variable) dipoles $\{\boldsymbol{\mu}_{i=1,N}\}$ of the melt ions, with i referring to a melt ion and j to an electrode atom. The interaction tensors T_{ij}^0 and $\mathbf{T}_{ij}^1$ are the normal charge–charge and charge–dipole interaction tensors to be evaluated in 2d periodic boundary conditions by the Ewald method. In addition to these electrostatic interactions we include in the potential a short-range contribution to the induction of dipoles on the melt ions, represented by the term $\mathbf{F}_{ij}^{\mathrm{sr}} \cdot \boldsymbol{\mu}_i$, which we will discuss in more detail below. In addition to these melt-electrode terms the total potential includes interactions between the charges and dipoles of the melt ions themselves, represented by the term V_{MM}, and the coulomb interactions between the charges of the electrode atoms, V_{EE} [3]. Finally, the potential involves two 'self-energy' terms $V_{\mathrm{M}}^{\mathrm{self}}(\{\boldsymbol{\mu}_{i=1,N}\})$ and $V_{\mathrm{E}}^{\mathrm{self}}(\{q_{j=1,M}\})$ which include the energy involved in developing dipoles on the melt ions and charges on the electrode atoms. The simulations work by requiring that at each configuration the

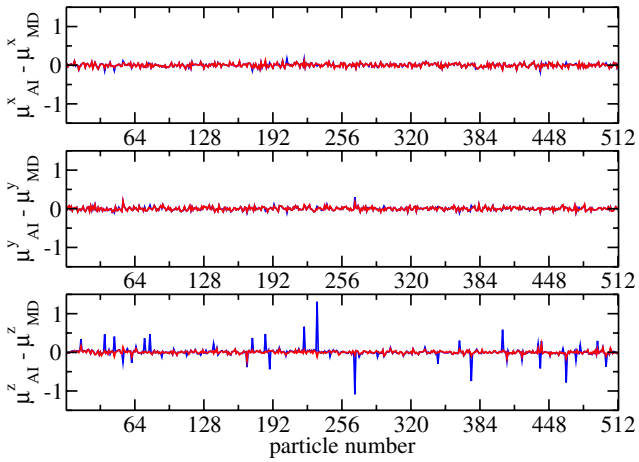

Figure 2. The difference between the dipoles on the chlorine atoms and those obtained from the *ab initio* calculations is indicated for all three x, y, and z coordinates from several configurations of the training set. Blue (dark) line: no short-range term included in V, red (light) line: short-range term $\mathbf{F}^{\rm sr}_{ij} \cdot \boldsymbol{\mu}_i$ included in V. The inclusion of this term only affects the z component of the dipole on the chlorine atoms situated at the interface.

total potential V is simultaneously minimized with respect to all the dipoles and charges; this is achieved by a conjugate-gradient procedure. These optimum dipoles and charges may then be used to calculate forces on the ions by invoking the Hellmann–Feynman theorem, in an analogous manner to the way the electronic degrees of freedom are treated in a Car–Parrinello simulation.

That there is a dipole moment induced on ions close to a metallic surface due to short-range interactions associated with the overlap of the electron densities of metal and ion is known from surface science and aqueous solution electrochemistry measurements [24]. The necessity for such a term in our context is illustrated in figure 2, where we show the difference between the *ab initio* values for the dipoles on the melt ions with those evaluated from the classical simulation for the same ionic configuration *with and without the short-range term*, $\mathbf{F}^{\rm sr}_{ij} \cdot \boldsymbol{\mu}_i$, *included in* V. In this comparison $V_{\rm MM}$ contains the polarization contributions to the melt–melt interaction potential which have been previously optimized (by force-matching on the basis of similar *ab initio* calculations) for bulk LiCl [12]. For the polarizabilities of the Cl^- ions, which enter $V^{\rm self}_{\rm M}(\{\boldsymbol{\mu}_{i=1,N}\})$, we use a value of 20.0 au, itself determined in condensed-phase electronic structure calculations [25]. The figure illustrates the differences in the components of the dipole moments on each Cl^- ion in the simulation (versus the ion label) taken from the *ab initio* and classical calculation. The dipoles in the classical calculation are induced by interactions with all other melt ions, as represented in $V_{\rm MM}$, and with the charges of the electrode atoms (i.e. they include the effects of all image–charge interactions with the electrodes) for the first set of data (blue line). The representation of the *ab initio* dipoles by the classical calculations is uniformly good for the x and y components and for most of the z components (perpendicular to the surface) except for a small number of ions which are close to the electrode surfaces; these correspond to the peaked points on figure 2. We attribute these discrepancies to a short-range interaction between the electrode and melt ions which we will model by parametrizing a suitable form for the function $\mathbf{F}^{\rm sr}$ in equation (5).

$\mathbf{F}^{\rm sr}$ behaves like an electric field which distorts the charge cloud of a melt ion due to overlap-mediated interactions with the electrode atoms. It might be expected to increase sharply with decreasing distance between them but, after some experimentation, we have chosen to represent it with the function

$$\mathbf{F}^{\rm sr}(\mathbf{r}_{ij}) = \hat{\mathbf{r}}_{ij} A \mathrm{e}^{-\alpha(r_{ij}-d)^2}, \tag{6}$$

where $\hat{\mathbf{r}}_{ij}$ is a unit vector. $\mathbf{F}^{\rm sr}(\mathbf{r}_{ij})$ is therefore directed along the interatomic separation and increases with decreasing r_{ij} for $r_{ij} > d$: as we shall see, d will be chosen to be smaller than the closest distance of approach allowed by the repulsive interactions between the ions and the electrode surface so that the non-intuitive decrease of $\mathbf{F}^{\rm sr}(\mathbf{r}_{ij})$ for $r_{ij} < d$ is never relevant. The reason for not choosing a monotonically increasing function of decreasing r_{ij} is that we found that such a representation led to instabilities in our simulations.

Values for A, α, and d were obtained by minimizing the objective function

$$O_{\rm P}(\{\chi_{\rm P}\}) = \sum_{C=1}^{N_{\rm config}} \sum_{i=1}^{N_{\rm anion}} \frac{|\boldsymbol{\mu}_i^{C,ai} - \boldsymbol{\mu}_i^{C}(\{\chi_{\rm P}\})|^2}{N_{\rm anion} N_{\rm config} |\boldsymbol{\mu}_i^{C,ai}|^2} \tag{7}$$

by varying the set of parameters $\{\chi_{\rm P}\}$ (i.e. A, α, and d). The index i runs over all the polarizable anions and the index C labels the ionic configuration on which *ab initio* and classical values are compared. $\boldsymbol{\mu}_i^{C}\{\chi_{\rm P}\}$ is the dipole calculated (with self-consistent charges and dipoles) from the model for ion i in configuration C with the parameter set $\{\chi_{\rm P}\}$, and $\boldsymbol{\mu}_i^{C,ai}$ is the corresponding *ab initio* value. For a single configuration of the system with 64 LiCl molecules, the sum over i and the components of the dipoles involves 192 terms; in practice the dipole and force-matching processes described within this section were carried out iteratively with the potential refined from the first set of *ab initio* calculations to generate 10 further configurations. The final optimization therefore involved 2112 terms in the sums of equation (7). A simplex procedure [26] is used to minimize the objective function. After this optimization process, the discrepancies between the *ab initio* and classical dipoles have been substantially reduced, as illustrated in figure 2, where the set of data obtained with the modified potential appear in red.

2.2. Representation of the ion–electrode short-range interactions

The remaining parts of the interaction between the electrode and melt atoms, in the absence of charge-transfer, consist of a repulsion due to the overlap of the ionic electron density with the valence electrons of the metal and an attractive dispersion term. We chose to model these effects with a simple pair potential of the same form as used to represent the ion–ion terms, i.e.

$$V^{\rm SR}_{\rm EM} = \sum_{i=1,N} \sum_{j=1,M} \left(B \mathrm{e}^{-\beta r_{ij}} - \frac{C_6 f_6(r_{ij})}{r_{ij}^6} - \frac{C_8 f_8(r_{ij})}{r_{ij}^8} \right). \tag{8}$$

Table 1. The fitted parameters for the Born–Mayer pair potential. All values are in atomic units. (Note: $A = 1.221\,34 \times 10^{-2}$; $\alpha = 3.338\,53 \times 10^{-1}$; $d = 3.688\,18$).

Interaction	β	B	C^6	C^8	f^6	f^8
Cl–Cl	1.591 65	$1.151\,44 \times 10^{2}$	$1.448\,98 \times 10^{2}$	$1.000\,13 \times 10^{2}$	1.683 48	1.646 84
Cl–Li	1.916 89	$5.477\,17 \times 10^{1}$	$9.853\,40 \times 10^{-4}$	$8.363\,47 \times 10^{-4}$	1.492 21	9.245 43
Cl–wall	2.783 05	$2.954\,20 \times 10^{4}$	$2.261\,10 \times 10^{2}$	$7.795\,63 \times 10^{2}$	2.484 66	2.500 97
Li–Li	5.854 31	$4.745\,50 \times 10^{1}$	$1.010\,10 \times 10^{-3}$	$1.006\,90 \times 10^{-3}$	6.437 58	1.705 98
Li wall	3.324 41	$7.287\,49 \times 10^{4}$	$4.200\,76 \times 10^{-1}$	3.407 48	9.691 27	7.116 26

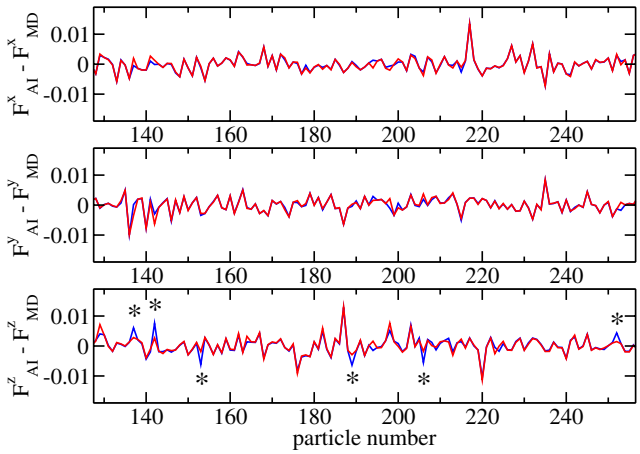

Figure 3. The difference between the forces on the chlorine atoms and those obtained from the *ab initio* calculations is indicated for all three x, y, and z coordinates from one of the configurations of the training set. Blue (dark) line: no short-range term included in V, red (light) line: short-range term $V_{\mathrm{EM}}^{\mathrm{SR}}$ included in V.

In practice other forms, such as a Morse potential, could also have been used. The f_6 and f_8 functions are Tang–Toennies damping functions which contain a single parameter—the (inverse) range at which the asymptotic forms of the dispersion terms are suppressed.

We illustrate the significance of these terms in the same fashion as above. Figure 3 shows the difference between the *ab initio* forces on the ions and those predicted by a classical calculation on the same configuration *when the* $V_{\mathrm{EM}}^{\mathrm{SR}}$ *terms are omitted or not from the classical calculation* (only one configuration is given here for reasons of clarity, but equivalent results were obtained for the other configurations). In the first case, corresponding to the blue line on the figure, the ions are then experiencing just the ion–ion interactions as described by the previously fitted interaction potential [12], and all the polarization effects arising from the interaction between their charges and dipoles and the electrode atoms. It can be seen that there are several ions lying close to the electrode surface, indicated by asterisks, where there is a large discrepancy between two sets of forces. We therefore perform a force-matching process for which the objective function is

$$O_{\mathrm{F}}(\{\chi\}) = \sum_{i=1}^{N_{\mathrm{melt}}} \sum_{C=1}^{N_{\mathrm{config}}} \frac{|\mathbf{F}_i^{C,ai} - \mathbf{F}_i^{C}(\{\chi\})|^2}{N_{\mathrm{melt}} N_{\mathrm{config}} |\mathbf{F}_i^{C,ai}|^2} \qquad (9)$$

which is a function of the set $\{\chi\}$ of short-range melt–wall potential parameters in equation (8). $\mathbf{F}_i^{C,ai}$ denotes the force on ion i in the *ab initio* calculation on configuration C, and $\mathbf{F}_i^{C}(\{\chi\})$ is predicted from the classical calculation with parameters $\{\chi\}$ for the same configuration. After minimization of this function, the agreement of *ab initio* and classical forces is improved as illustrated from the red line on figure 3, so that the discrepancy for ions close to the electrode surface is similar to that for ions which are remote from it; the latter arise from imperfections in the bulk ion–ion potential.

The final optimization involved 4224 terms in the sums in equation (9). The final value of O_{P} was 0.0507, which indicates an excellent representation of the dipoles, and for $O_{\mathrm{F}} = 0.141$ which is slightly worse than is obtained for the fit to bulk LiCl with the bulk potential used here. The final sets of parameters are given in table 1.

3. Interfacial structure in the Al/LiCl system

3.1. Molecular dynamics simulations

Several classical simulations of the Al electrode–LiCl melt simulation have been made for differing values of the applied electrode potential difference in order to examine the potential dependence of the melt structure at the interface. The simulations were carried out on considerably larger systems than those prepared for input to the *ab initio* calculations. The melt region included 500 Li^+ and 500 Cl^- ions and the electrodes included 432 *fixed* Al atoms arranged, as before, in an fcc structure with the (100) surface exposed to the melt. The dimensions of the cell were 24.297 Å in the x and y directions, and 49.8345 Å between the innermost layer of electrode atoms along z. The x and y distances were chosen to match a number of 6 fcc Al unit cells and the simulations were initiated by taking a melt configuration from a bulk liquid LiCl simulation in which the cell dimensions had been matched to these values. The simulation was then run for 100 ps to allow for equilibration and this was followed by 75 ps of production runs. The simulations with different applied potentials were initiated in sequence and an equilibration period of 60 ps was allowed before collecting statistics. The applied potential differences $|\Psi^+ - \Psi^-|$ investigated were 0.0, 0.1, 0.2, 0.5, 1.0, 1.5, 2.0, 3.0, 4.0 and 5.0 V.

3.2. Ion density profiles

Figure 4 shows the profiles of the density of Li^+ and Cl^- ions across the simulation cell for various values of the applied potential. As viewed, a positive potential (Ψ^+) is applied to the left-hand electrode (the anode) and an equal and opposite negative potential to the right-hand electrode, so that the total

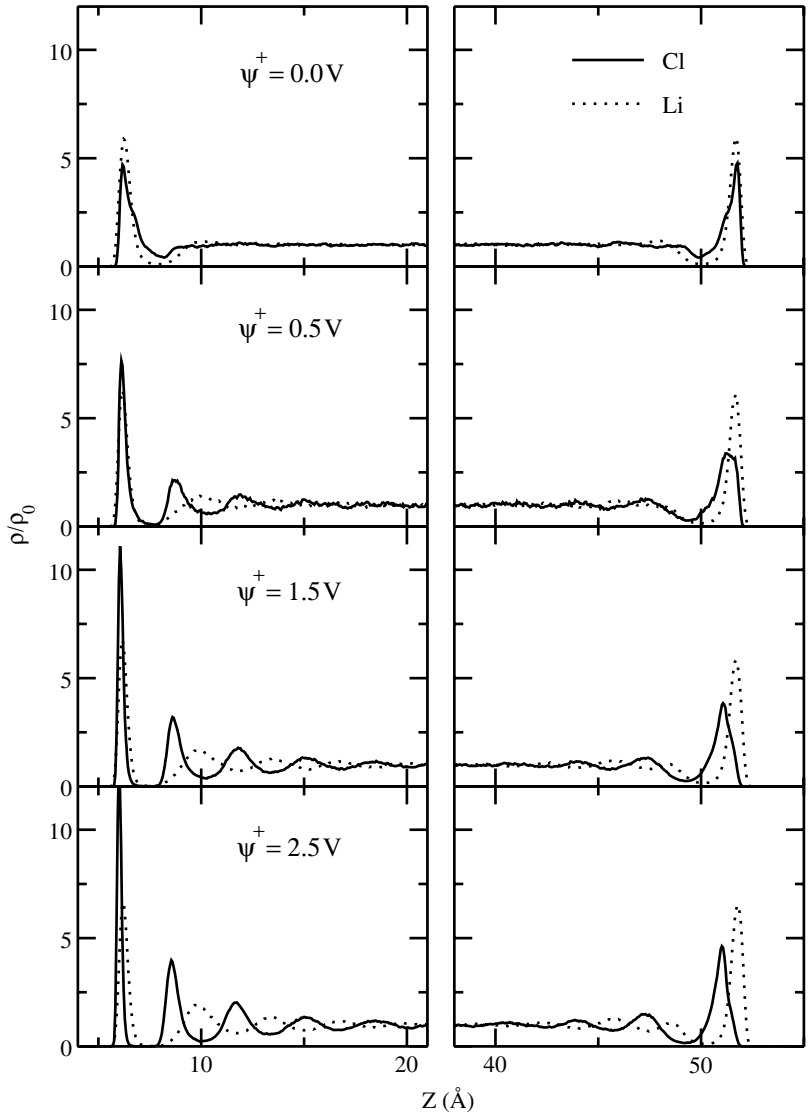

Figure 4. Ionic density profiles across the simulation cell for different values of the applied potential difference. The electrode set at a positive potential (Ψ^+) is located at the left end of the simulation cell. ρ_0 is the bulk melt density.

potential drop across the 'cell' (v.i.) is twice Ψ^+. For $\Psi^+ = 0$, a layer of weakly bound ions forms at the electrode surfaces and both species are seen, from the depth of the minimum separating this layer from the remaining fluid, to be in reasonably fast exchange with ions in the bulk. Beyond the first layer there is a weak tendency for the anion and cation densities to oscillate out of phase. Note that ionic densities do not exhibit an electrical double-layer in the conventional sense. The features observed here are much more complex, due to the strong interactions between differently charged ions. This has already been observed in various computational studies of the interfacial properties of ionic liquids [1–3, 5, 6].

As the applied potential is increased, different behaviours are observed for the interfacial structure at the two electrodes. At the anode, the Cl^- ions are very strongly adsorbed and they drag the Li^+ ions with them; the depth of the minimum in the density profile increases, suggesting that exchange with the bulk is slowed markedly. The application of the potential increases the amplitude of the out-of-phase oscillations in the densities of the two species. The cathode behaves differently; here the Li^+ ions remain in a relatively loosely held surface layer but the Cl^- ions are pushed out towards the bulk, creating a strongly polarized but apparently more fluid adsorbed film. In previous work on KCl [1], where the two ions were of very similar size and were not polarizable, the polarization of the two interfaces was much more symmetrical. In their study of a room temperature ionic liquid (RTIL) confined between two electrified walls, Pinilla *et al* also observed differences between positively and negatively charged walls [2]. In that case, the system consisted in dimethylimidazolium cations, which are molecular species and therefore have some orientational degrees of freedom, and chloride anions (for which polarization effects were neglected). On the negatively charged electrode, both species were adsorbed at the interface in the same layer, while for the positively charged electrode, the increase of the surface charge led to a closer approach of Cl^- ions only, inducing some kind of segregation. This is the opposite to what we report here;

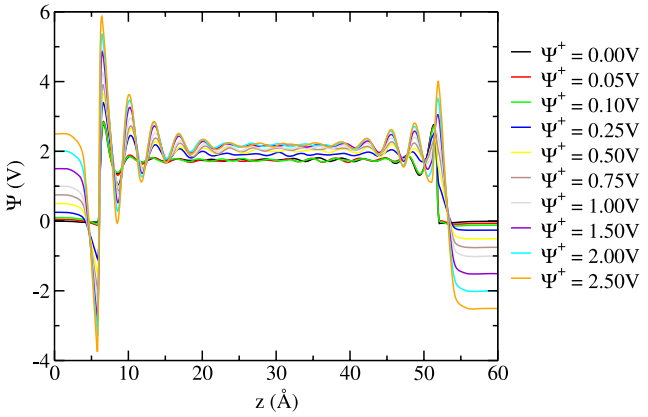

Figure 5. Electrostatic potential profile across the simulation cell. As a convention we take $\Psi^+ = -\Psi^- = \frac{1}{2}|\Psi^+ - \Psi^-|$.

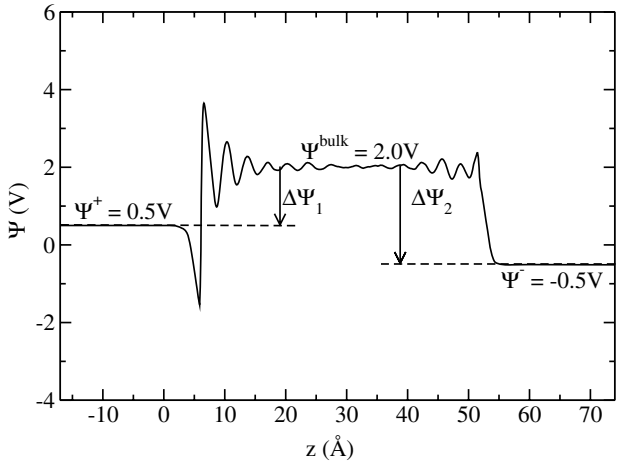

Figure 6. Graphical explanation of the notation introduced in the text for an applied potential $|\Psi^+ - \Psi^-|$ of 1.0 V. The potential reaches a value of $\Psi^{\text{bulk}} = 2.0$ V in the bulk liquid. Two metal/molten salt interfaces are then defined: at the left-hand electrode the potential difference $\Delta\Psi_1 = \Psi^+ - \Psi^{\text{bulk}}$ is −1.5 V, while on the right-hand side $\Delta\Psi_2 = \Psi^- - \Psi^{\text{bulk}}$ equals −2.5 V.

in LiCl the anion is the larger ion and also is the one which is polarizable and interacts most strongly with the electrode surface. The distinct behaviour observed between the two electrodes therefore reflects the important differences in size and polarizabilities of the two ionic species in the melt.

3.3. Electrostatic potential profile

The electrostatic potential across the simulation cell $\Psi(z)$ includes two contributions:

$$\Psi(z) = \Psi_q(z) + \Psi_{\boldsymbol{\mu}}(z), \tag{10}$$

where the first term originates from the ionic and metallic charge distribution:

$$\Psi_q(z) = \Psi_q(z_0) - \frac{1}{\epsilon_0}\int_{z_0}^{z} \mathrm{d}z' \int_{-\infty}^{z'} \mathrm{d}z''\, \rho_q(z''), \tag{11}$$

and the second term is the contribution from the induced dipoles:

$$\Psi_{\boldsymbol{\mu}}(z) = \Psi_{\boldsymbol{\mu}}(z_0) + \frac{1}{\epsilon_0}\int_{z_0}^{z} \mathrm{d}z'\, \rho_{\boldsymbol{\mu}}(z'). \tag{12}$$

The profiles obtained by taking z_0 to be a reference point inside the left-hand electrode, where $\Psi_q(z_0 < 0) = \Psi^+$ and $\Psi_{\boldsymbol{\mu}}(z_0 < 0) = 0.0$ V, are displayed on figure 5. In the centre of the cell the potential is constant, due to the screening of the charges of the electrodes by the (ionically conducting) melt. Very strong oscillations are obtained near the interfaces; those are mainly due to the out-of-phase oscillations of the densities of oppositely charged ions. A layer of 5–13 Å is necessary to screen completely the electrode potential and reach an in-bulk Ψ^{bulk} value for the potential. Three régimes are observed for Ψ^{bulk}. For some null or very weak applied potentials, the same value of ≈1.75 V is obtained. Then, for $\Psi^+ - \Psi^- > 0.5$ V, a progressive shift of this potential appears, until a new almost constant value of $\Psi^{\text{bulk}} \approx 2.16$ V is obtained for $\Psi^+ - \Psi^- > 3.0$ V.

Each metal/melt interface can be viewed as a parallel plate capacitor, with a potential drop between the two plates given by $\Delta\Psi = \Psi^{\pm} - \Psi^{\text{bulk}}$ and an accumulated charge on a given plate equal to the sum of all the charges carried by the metallic electrode atoms (the various notations introduced are summarized in figure 6). The variation of the surface charge σ with $\Delta\Psi$ is given in figure 7, with two points for each simulation because of the existence of two distinct interfaces. The value of $\Delta\Psi$ has some imprecision due to the oscillations in Ψ^{bulk} on figure 5, this is about the size of the points on the graphic.

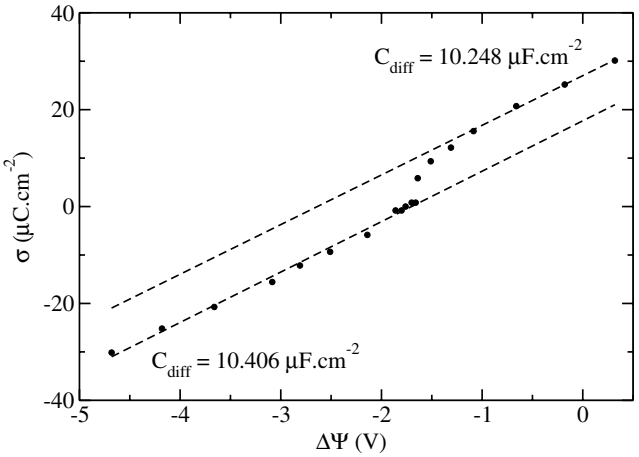

Figure 7. Variation of the surface charge with the potential drop across the interface $\Delta\Psi = \Psi^{\pm} - \Psi^{\text{bulk}}$.

The first quantity that can be evaluated from this plot is the potential of zero charge (PZC), $\Delta\Psi_{\text{PZC}} = -1.76$ V. This seems like a large value compared to experimentally measured quantities, however one must remember that the experimental quantity is always measured with respect to a reference electrode, whereas we are dealing with absolute potentials. In our calculations the potential drops very rapidly across the region between the surface layer of electrode atoms,

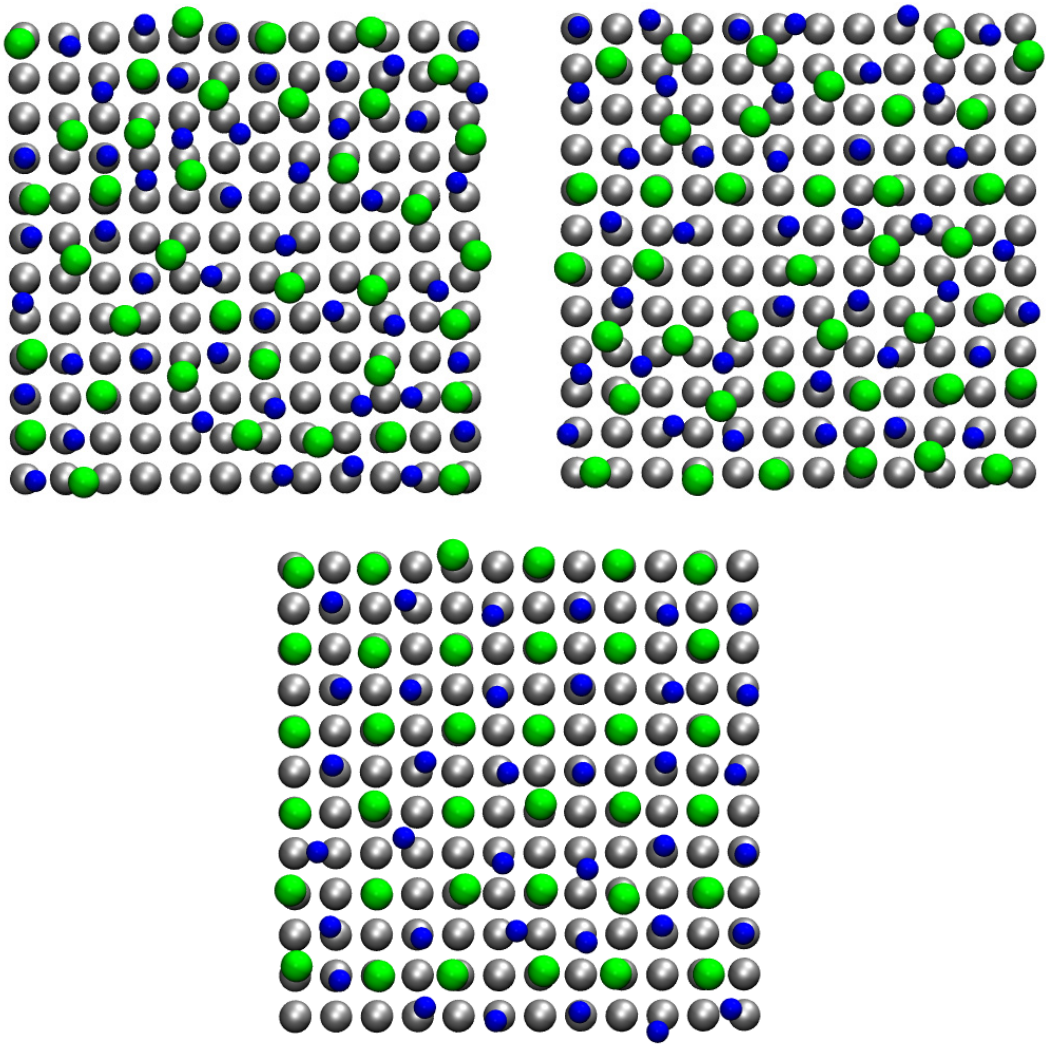

Figure 8. Snapshots of the adsorbed layer on the metal surface. From top to bottom, $\Psi^- = -2.5$ V, $\Psi^+ = 0.0$ V and $\Psi^+ = 2.5$ V. Green (light): Cl^- ions, blue (dark): Li^+ ions, grey: Al atoms.

where the electrode charges are located, and the first layer of melt ions. In a real metallic surface, the valence electron density of the metal would extend out into this region and contribute to a partial screening of the electrode charges, giving a different character to the potential across this gap [27]. If we were to use a reference electrode (with similar characteristics to the electrodes of our simulation model), this limitation of our representation of the metallic surface would not be evident in the PZC value.

Secondly, we may obtain values for the differential capacitance

$$C_{\text{diff}} = \frac{\partial \sigma}{\partial \Delta \Psi} \tag{13}$$

which can be extracted by differentiation of the surface charge with respect to the potential difference across the interface, as shown in figure 7. Three patterns can be distinguished: on the two outer parts of the curve, almost constant differential capacitances of 10.406 and 10.248 μF cm^{-2} are obtained. The most negative of the potential differences occur at the right-hand electrode, where the corresponding ion density profiles are shown in the right-hand side of figure 4. Between the two regions of constant slope in the σ versus $\Delta\Psi$ figure, at potential differences slightly less negative than the PZC, a sudden increase of the surface charge with $\Delta\Psi$ is observed. This corresponds to a maximum for the differential capacitance.

3.4. Structure of the adsorbed layer

The steep rise in the surface charge density (and the corresponding peak in the differential capacitance) is caused by a change in the structure of the adsorbed layer of ions at the anode (left-hand electrode) as the potential applied to the electrode is increased. Referring to the ion density profiles in figure 4, it occurs for applied potentials between $\Psi^+ = 0.5$ V and 1.5 V in the panels on the left-hand side of the figure. Some typical snapshots of the adsorbed layer for different potential drops are given on figure 8. The first two snapshots correspond to potential drops before and exactly at the PZC. In both cases, the arrangements of the ions are disordered. In the final snapshot, which corresponds to a potential drop less

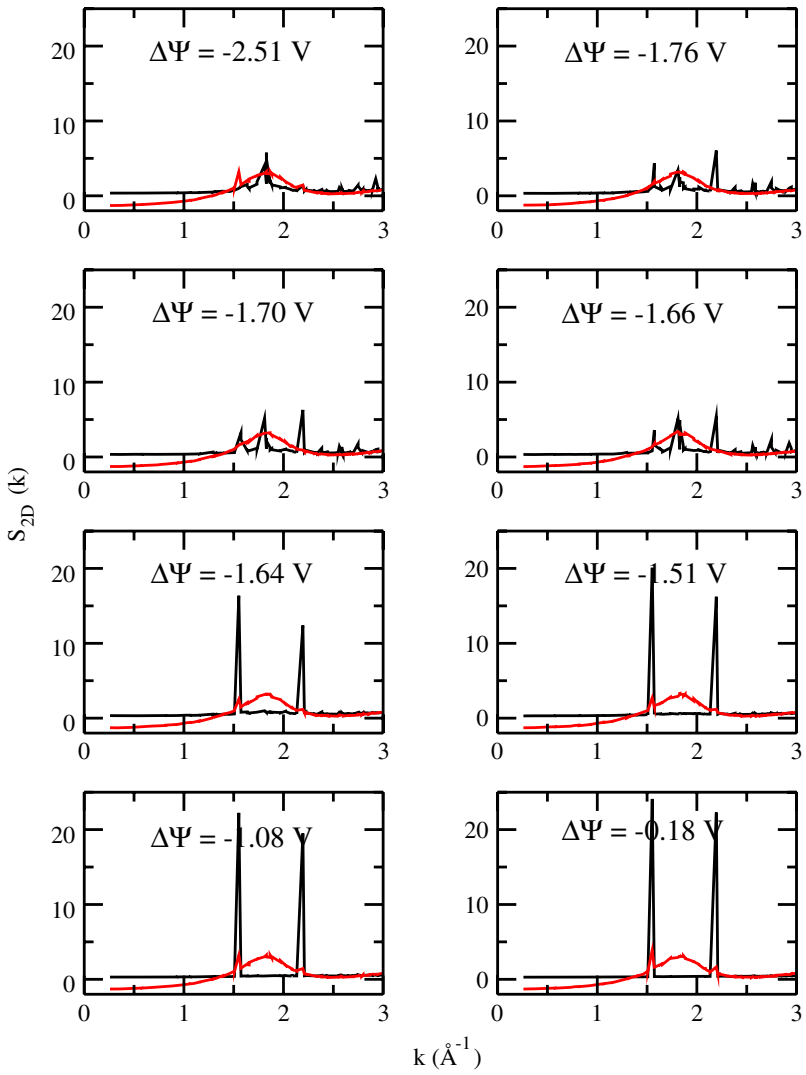

Figure 9. In-plane Cl^-–Cl^- structure factor for various potential drops across the metal/molten salt interface. Black: adsorbed layer, red: liquid slice between the adsorbed layer on each electrode.

negative than the PZC, a significant ordering of both ions is observed with the ions appearing to be bound to the hollow sites of the aluminium surface.

In order to assign a potential to the transition between the disordered and ordered states of the adsorbed layer we have computed the in-plane partial structure factors for different applied potentials. The Cl^-–Cl^- partial structure factors for atoms in the adsorbed layer and in the adjacent layer of liquid for wavevectors in the plane of the surface are shown in figure 9. A structural transition in the adsorbed layer is clearly observed: for $\Delta\Psi$ values more negative than -1.66 V only weak features are seen in the structure factor whereas for $\Delta\Psi$ values higher than -1.64 V, two sharp and very intense Bragg peaks are observed, which correspond to the $\mathbf{k} = \frac{2\pi}{a}(1, 0)$ and $\frac{2\pi}{a}(1, 1)$ scattering vectors, where a is the lattice parameter of the aluminium metal ($a = 4.0495$ Å). This abrupt change in the interfacial structure is therefore responsible for the sharp increase in the surface charge density and the maximum we observe in the differential capacitance just after the PZC. A similar potential-induced structural transition in the adsorbed layer of an ionic liquid was observed by Freyland *et al* using *in situ* STM [28, 29]. The structure factors for the layers of liquid adjacent to the adsorbed layer are more liquid-like, though they do exhibit small peaks at the positions of the Bragg peaks, showing that the lateral ordering effect imposed by the atomic structure in the Al surface does propagate out into the liquid. (Recall, however, that the surface atoms are fixed in our simulations, so that the effect may be more exaggerated than in a physical system.)

Away from the sharp rise close to the PZC, the surface charge density increases linearly with $\Delta\Psi$, indicating that the differential capacitance is independent of the applied potential (figure 7) in these regions of applied potential. The fact that the interfacial capacitance is potential-independent in these regions deserves further comment, as mean-field treatments of the capacitance of the double-layer in electrolyte solutions suggest that it should vary with the square-root of the potential drop across the interface [4]. A constant capacitance is the behaviour expected for a dielectric and it is tempting to suggest that we see this behaviour because of the electronic

polarization of the Cl^- ions close to the electrode surface (which is not accounted for in the mean-field treatments, nor in any previous simulation study [4–6]). It is certainly true that the induced dipoles make a substantial contribution to the interfacial potential drop, however, as figure 4 shows there is also a substantial reorganization of the ionic positions as the applied potential is varied. We will investigate this point further in future work. The fact that the slopes for high and low potential drop are almost equal we believe to be an accidental feature of this particular system as the interfacial structures across which the capacitance is being measured are very different and there is no physical reason why they should polarize at the same rate. The way that the change in potential influences the ion density profiles is shown in figure 4. The most negative $\Delta\Psi$ values correspond to the negatively charged electrode surface which corresponds to the density profiles appearing in the right side of the figure, where the polarization of this interface is associated with the anions being progressively pushed away from the surface as the applied potential is increased. $\Delta\Psi$ values less negative than the PZC are associated with the ordered layer at the left-hand electrode where the relative displacement of the density profiles of cations and anions is less marked.

4. Summary

We have demonstrated the feasibility of parametrizing potentials to describe the interactions of ions with metallic walls directly from planewave DFT electronic structure calculations by an extended 'force-matching' procedure. The ability of a DFT description of this type to represent molecule–metal interactions was recently tested [20]. A well-known shortcoming of simple generalized gradient functionals is an underestimate of the dispersion (van der Waals) interactions [30] which might lead to an underestimate of the strength of the attractive interactions between the Cl^- ions and the metal surface. We note that more advanced functionals which include the dispersion interactions are under development [31] which we will use in future work. The interaction potential includes the polarization of the ions by interionic interactions and by the interfacial potential and the polarization of the metal by the interactions with the charges and induced dipoles of the ions in the interfacial region; such effects have not been incorporated in previous simulation studies of ionic liquids at interfaces. We used the potentials to conduct simulations of the LiCl/Al system, in which the positions of the Al atoms were held fixed, at various values of the applied electrical potential. The interfacial structure was strongly affected by the applied potential and we observed a potential-induced phase transition in the first layer of ions adsorbed on the surface. This was associated with a peak in the interfacial capacitance of a type very similar, though sharper, to that seen in experimental studies of RTILs [32]. At potentials away from the phase transition the capacitance was found to be independent of the applied potential, a finding which will be the subject of further work.

Acknowledgments

We would like to acknowledge the PCR ANSF of the PACEN programme (CNRS) and the EPSRC (GR/T23268/01) for financial support. Sami Tazi is beneficiary of a fellowship from UPMC—Fondation pour les Energies de Demain—Institut de France.

References

[1] Lanning O and Madden P A 2004 Screening at a charged surface by a molten salt *J. Phys. Chem.* B **108** 11069–72
[2] Pinilla C, Del Popolo M G, Kohanoff J and Lynden-Bell R M 2007 Polarization relaxation in an ionic liquid confined between electrified walls *J. Phys. Chem.* B **111** 4877–84
[3] Reed S K, Lanning O J and Madden P A 2007 Electrochemical interface between an ionic liquid and a model metallic electrode *J. Chem. Phys.* **126** 084704
[4] Kornyshev A A 2007 Double-layer in ionic liquids: paradigm change? *J. Phys. Chem.* B **111** 5545–57
[5] Fedorov M V and Kornyshev A A 2008 Ionic liquid near a charged wall: structure and capacitance of electrical double layer *J. Phys. Chem.* B **112** 11868–72
[6] Fedorov M V and Kornyshev A A 2008 Towards understanding the structure and capacitance of electrical double layer in ionic liquids *Electrochem. Acta* **53** 6835–40
[7] Siepmann J I and Sprik M 1995 Influence of surface-topology and electrostatic potential on water electrode systems *J. Chem. Phys.* **102** 511–24
[8] Reed S K, Madden P A and Papadopoulos A 2008 Electrochemical charge transfer at a metallic electrode: a simulation study *J. Chem. Phys.* **128** 124701
[9] Willard A P, Reed S K, Madden P A and Chandler D 2009 Water at an electrochemical interface—a simulation study *Faraday Discuss.* **141** 423–41
[10] Aguado A, Bernasconi L, Jahn S and Madden P A 2003 Multipoles and interaction potentials in ionic materials from planewave-DFT calculations *Faraday Discuss.* **124** 171–84
[11] Salanne M, Simon C, Turq P and Madden P A 2007 Conductivity-viscosity-structure: unpicking the relationship in an ionic liquid *J. Phys. Chem.* B **111** 4678–84
[12] Ohtori N, Salanne M and Madden P A 2009 Calculations of the thermal conductivities of ionic materials by simulation with polarizable interaction potentials *J. Chem. Phys.* **130** 104507
[13] Heaton R J, Brookes R, Madden P A, Salanne M, Simon C and Turq P 2006 A first-principles description of liquid BeF_2 and its mixtures with LiF: 1. potential development and pure BeF_2 *J. Phys. Chem.* B **110** 11454–60
[14] Salanne M, Simon C, Turq P and Madden P A 2009 Heat-transport properties of molten fluorides: determination from first-principles *J. Fluorine Chem.* **130** 38–44
[15] Salanne M, Simon C, Groult H, Lantelme F, Goto T and Barhoun A 2009 Transport in molten LiF–NaF–ZrF_4 mixtures: a combined computational and experimental approach *J. Fluorine Chem.* **130** 61–6
[16] Pounds M A 2009 Electrochemical charge transfer at a metallic electrode: a simulation study *PhD Thesis* University of Edinburgh
[17] The CPMD consortium *CPMD Version 3.x* http://www.cpmd.org MPI Für Festkörperforschung and the IBM Zurich Research Laboratory
[18] Perdew J P, Burke K and Ernzerhof M 1996 Generalized gradient approximation made simple *Phys. Rev. Lett.* **77** 3865–8

[19] Troullier N and Martins J L 1991 Efficient pseudopotentials for plane-wave calculations *Phys. Rev.* B **43** 001993
[20] Fernández-Torre D, Kupiainen O, Pyykkö P and Halonen L 2009 Long-range interactions between polar molecules and metallic surfaces: a comparison of classical and density functional theory based models *Chem. Phys. Lett.* **471** 239–43
[21] Silvestrelli P L, Marzari N, Vanderbilt D and Parrinello M 1998 Maximally-localized Wannier functions for disordered systems: application to amorphous silicon *Solid State Commun.* **107** 7–11
[22] Silvestrelli P L 1999 Maximally localized Wannier functions for simulations with supercells of general symmetry *Phys. Rev.* B **59** 9703–6
[23] Humphrey W, Dalke A and Schulten K 1996 VMD—visual molecular dynamics *J. Mol. Graph.* **14** 33–8
[24] Magnussen O M 2002 Ordered anion adlayers on metal electrode surfaces *Chem. Rev.* **102** 679–726
[25] Fowler P W and Madden P A 1984 In-crystal polarizabilities of alkali and halide ions *Phys. Rev.* B **29** 1035–42
[26] Press W H, Flannery B P, Teukolsky S A and Vetterling W T 1992 *Numerical Recipes* 2nd edn (Cambridge: Cambridge University Press)
[27] Price D L and Halley J W 1995 Molecular dynamics, density functional theory of the metal–electrolyte interface *J. Chem. Phys.* **192** 6603–12
[28] Pan G-B and Freyland W 2006 2D phase transition of PF_6 adlayers at the electrified ionic liquid/Au(1 1 1) interface *Chem. Phys. Lett.* **427** 96–100
[29] Freyland W 2007 Interfacial phase transitions in conducting fluids *Phys. Chem. Chem. Phys.* **10** 923–36
[30] Hult E, Rydberg H and Lundqvist B I 1999 Unified treatment of asymptotic van der Waals forces *Phys. Rev.* B **59** 4708–13
[31] Silvestrelli P L 2008 Van der Waals interactions in DFT made easy by Wannier functions *Phys. Rev. Lett.* **100** 053002
[32] Islam M M, Alam M T and Ohsaka T 2008 Electrical double-layer structure in ionic liquids: a corroboration of the theoretical model by experimental results *J. Phys. Chem.* C **112** 16568–74